THE UNIVERSITY OF ALABAMA IN HUNTSVILLE

FINAL REPORT

SIFTER: SCINTILLATING FIBER TELESCOPES FOR ENERGETIC RADIATION, GAMMA-RAY APPLICATIONS

NASA Grant NAG 5-5298

6/8/2000 – 6/30/2002

PREPARED BY WILLIAM S. PACIESAS

DECEMBER 5, 2002

INTRODUCTION

NASA Grant NAG 5-5298 provided funds for the research project "SIFTER: Scintillating Fiber Telescopes for Energetic Radiation, Gamma-Ray Applications" approved under the NASA High Energy Astrophysics Research Program. The principal investigator of the proposal was Prof. Geoffrey N. Pendleton, who is currently on extended leave from UAH. Prof. William S. Paciesas administered the grant during Dr. Pendleton's absence. The project was originally funded for one year from 6/8/2000 to 6/7/2001. Due to conflicts with other commitments by the PI, the period of performance was extended at no additional cost until 6/30/2002.

The goal of this project was to study scintillating fiber pair-tracking gamma-ray telescope configurations specifically designed to perform imaging and spectroscopy in the 5–250 MeV energy range. The main efforts were concentrated in two areas: 1) development of tracking techniques and event reconstruction algorithms, with particular emphasis on angular resolution; and 2) investigation of coded apertures as a means to improve the instrument angular resolution at low energies.

DEVELOPMENT AND VALIDATION OF TRACKING TECHNIQUES

We devoted much of our effort to the development of tracking techniques for scintillating fiber pair tracking detectors, including extensive detailed simulations, tracking algorithm development, and data analysis. We focused specifically on the angular resolution capabilities. We used our previously developed extensive set of simulation software tools based on the well-known GEANT3 code to simulate the performance of various fiber detector configurations. Example results are illustrated in Figure 1, which shows angular resolution estimates for a large scintillating fiber pair tracking system. The upper solid curve represents the 68% space containment angle while the dotted line represents the 95% space containment angle. The lower solid curve represents the 68% space containment angle for the 50% of the events selected as high quality by an automated algorithm developed by us that evaluates the estimated number of missing track hits and the straightness of the electron tracks to rank the events by quality. The large number of tracker planes allows us to perform these kinds of event selections to tune the response to different scientific objectives.

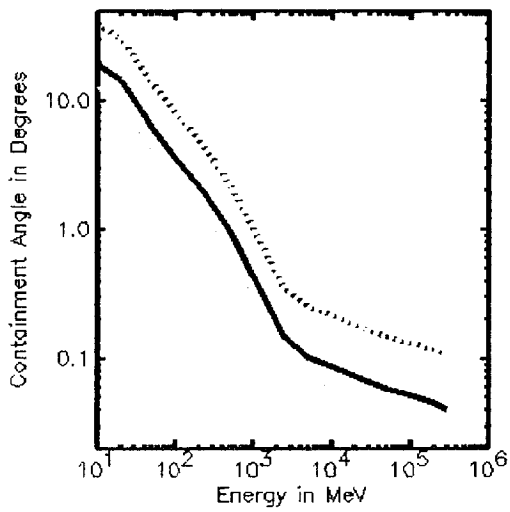

Figure1. Estimated angular resolution vs. photon energy for a large fiber tracking system.

We performed beam tests at the Center for Advanced Microstructures and Devices (CAMD) synchrotron facility using our fiber tracker prototype system to characterize the measured angular resolution of a fiber detector. The test apparatus consisted of 20 fiber planes, with a total of 1,280 active fiber/MAPMT channels. Each plane had orthogonal arrays of *x-y* fibers mounted below a tantalum converter foil, 0.0082 cm thick (0.02 radiation lengths). The beam test apparatus used a single discriminator per MAPMT anode, and the fibers were not optimized to reduce optical cross talk. The beam test data therefore represent a worst-case scenario for evaluating the effects of cross-talk on instrument performance.

Figure 2 shows the beam test apparatus. The test apparatus was exposed to a continuum of gamma-ray energies from ~50 MeV to 1.4 GeV. To estimate the incident photon energy, a large cylindrical NaI (Tl) scintillator (5 in. thick, 10 in. diameter) was operated behind the fiber tracker apparatus. The pulse-height to energy conversion of this scintillator was calibrated with atmospheric muons at 60 and 122 MeV.

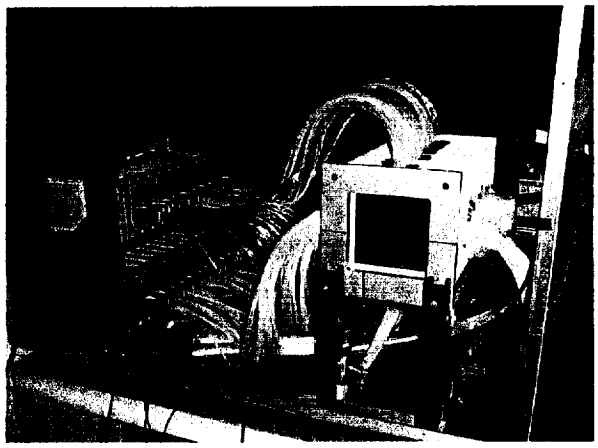

Figure 2. CAMD beam test apparatus using 20 MAPMTs to read out 20 fiber detector planes.

Simulations of the entire beam test setup show that energy deposited in the NaI provides an estimate of the incident photon energy with resolution of 20-25% (FWHM) over the beam energy range. The simulation results were used to correct the measured NaI data in order to present angular resolution results as a function of incident photon energy. Figure 3 shows a sample event from this study.

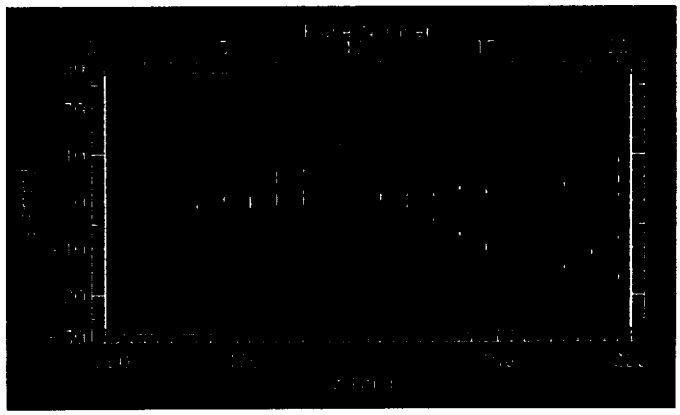

Figure 3. Gamma-ray event from beam test.

The system performed well, and pair tracking was demonstrated with reasonable performance. However, due to the misalignment of some fiber/MAPMT interfaces, and the use of fibers without extramural absorber (EMA), there was significantly more optical cross talk between the channels than expected. Furthermore, the system did not have individual discriminators for each channel, which led to increased noise in some channels and decreased fiber detection efficiency in others. These non-optimum conditions were useful for examining the effects of cross-talk and inefficiency on angular resolution, but they did not allow a representative demonstration of the true fiber telescope capability.

Although the CAMD instrument was not fully optimized in terms of its geometry, optical cross talk, readout noise, and fiber detection efficiency, we were able to use the beam test data to evaluate the pair tracking performance. Figure 4 shows a sample gamma-ray induced event from the beam test. Even with the non-optimized system, the fiber detectors performed well in tracking minimum ionizing particles. Using track reconstruction algorithms developed for FiberGLAST, we were able to compute the (normal incidence) angular response of the beam test instrument as a function of energy. The results are shown in Figure 4, compared to simulation results from the large FiberGLAST concept instrument (Pendleton et al. 1999). These results show that the system performance is nearly as good as expected from simulations. Comparison with the simulations indicates that the non-optimum cross-talk, noise, and fiber efficiency degrade the angular resolution and photon detection efficiency by ~10–20%.

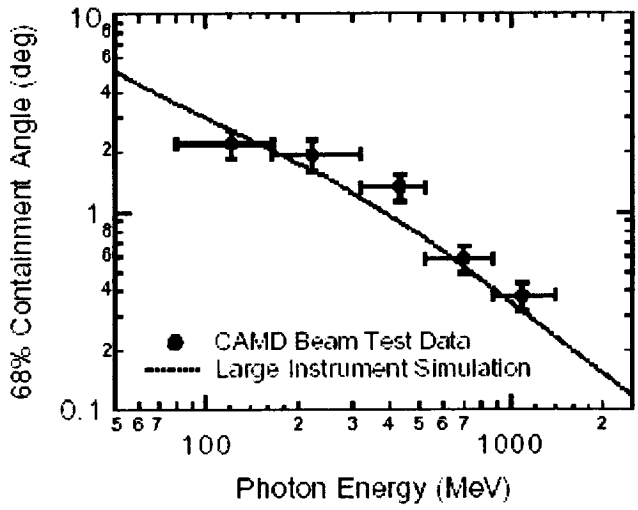

Figure 4. Measured angular resolution as a function of derived photon energy from the CAMD beam test instrument compared to simulations of a large area telescope.

CODED APERTURES

Application of coded-aperture techniques to high-energy gamma-ray detectors has been proposed as a way to greatly improve their angular resolution (Carter et al. 1982). In order to investigate this further, we performed simulations of a scintillating fiber telescope in combination with a coded mask.. The SIFTERCAM instrument concept is shown in Figure 5. The tracker consists of a 60 cm × 60 cm × 180 cm version of the SIFTER gamma-ray tracker instrument, referred to in

the figure as the "detector stack." The upper half of this detector stack is surrounded by an active mask consisting of high-Z material 2 r.l. thick with a 3 cm × 3 cm × 1.7 cm element size. The mask has one top plane and four side planes. The top plane is 90 cm × 90 cm and is positioned 20 cm above the top of the detector. The side planes are 90 cm × 110 cm and are positioned 15 cm out from the sides of the detector stack. The active mask is designed to veto cosmic-ray proton events that interact in the mask material and produce π^0 particles that decay to gamma-rays and could interact in the detector. In addition, events that produce high energy neutrons in the mask will trigger the active mask as well, eliminating this source of potential background.

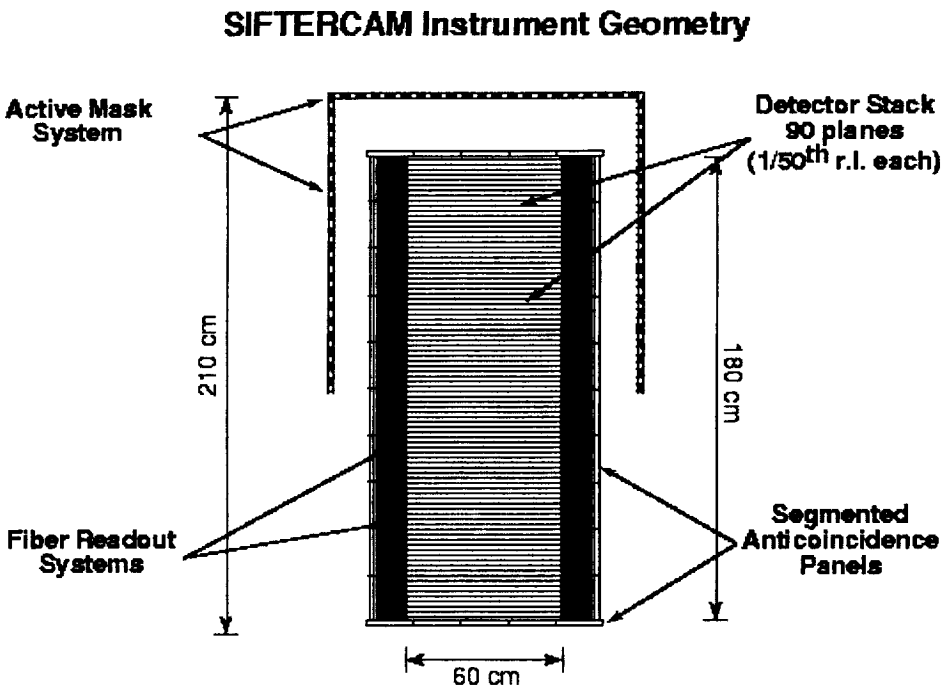

Figure 5. Schematic view of the SIFTERCAM instrument concept.

The detector stack is surrounded by a hodoscopic plastic scintillator anti-coincidence system similar to that developed during the FiberGLAST ATD effort (Pendleton et al. 1999). In the SIFTERCOM preliminary simulations, the mask is a simple checkerboard pattern, but the three dimensional volume of the detector stack produces a unique mask pattern for each source viewing direction.

Figure 6 shows a side view of the detector stack vertex density distribution for a plane wave of photons incident on the detector at an angle of 2° with respect to the detector normal. The lighter regions indicate the portions of the detector stack unshadowed by the mask where the photon pair conversion vertex density will be higher, on average. The darker areas represent the regions of the detector stack shadowed by the mask, as well as the regions deeper in the detector stack. Clearly the mask pattern will change as a strong function of source viewing angle. The pattern changes more rapidly as a function of source viewing angle in the deeper parts of the detector. Superimposed on the vertex density distribution is a white grid that shows how Monte Carlo simulation data are binned for the χ^2 tests used for the point source localizations for the masked geometry. The grid covers one shadowed and one open cell of the detector stack. Data from Monte Carlo simulations are folded into this bin cell grid for each adjacent pair of shadowed and open cell section of the detector stack.

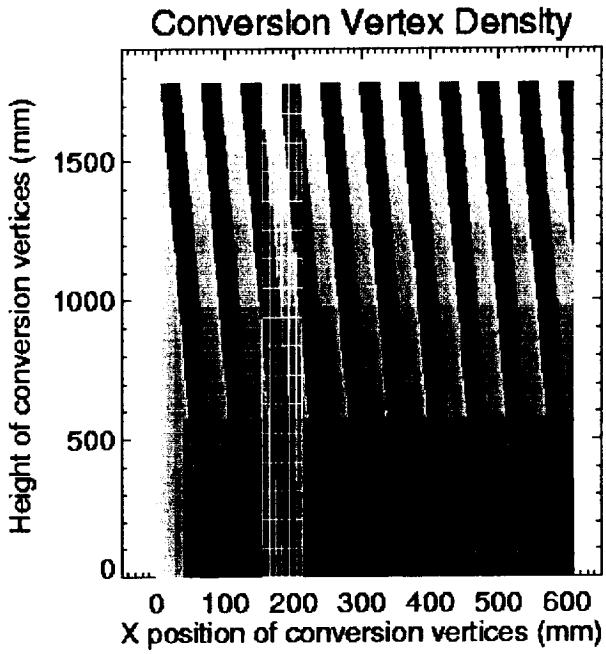

FIGURE 6. Conversion vertex density for a point source 2° from the detector normal.

Figure 7 shows the vertex density patterns in the binned cell grid format for the grid shown in Figure 6. The grey surface represents the binned vertex density pattern for a normally incident plane wave of photons, and the darker surface represents the binned vertex density for a uniform distribution of photons incident on the detector over an angular range of –10° to +10°. These patterns are clearly distinguishable—indicating the advantage of the mask system.

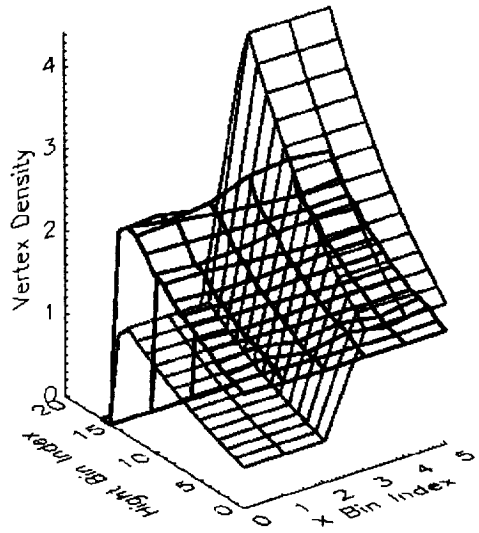

FIGURE 7. Conversion vertex density distributions for a point source (grey) and uniform distribution (black).

The point source resolution of both a masked and unmasked version of the SIFTERCAM detector stack were simulated using Monte Carlo techniques to compare the capabilities of each type of approach. A point source at 1% of the Galactic diffuse emission, using the values described above, was placed at -1.0° off the detector axis and superimposed on both the Galactic diffuse and atmospheric background. The simulations were run in a 2-dimensional scenario but will be extended to a three dimensional case in the concept study. For the unmasked system the detected flux values were increased by a factor of ~2 since the mask was not present. For the unmasked system, a maximum likelihood technique was employed, derived from techniques developed earlier (Jenkins et al. 1985). For the masked analysis, a χ^2 test was applied to the Monte Carlo data summed into the binning format shown in Figure 6. Then these data were fit with a χ^2 test using various detector mask patterns.

The results of these two tests are shown in Figure 8 for both the 10–30 MeV and 30–100 MeV energy ranges. Here, source positions are assumed from a range of directions around –1°, and the probability that the source comes for that direction is calculated. The probabilities are presented in units of log(probability) plus a constant, more appropriate for the maximum likelihood method. Larger values of log(probability) indicate better fits. For the χ^2 test using the masked data, the maximum probabilities correspond to roughly 50%, or a reduced χ^2 slightly less than 1. The maximum likelihood calculations using the unmasked data are shown in the top two panels of Figure 9 and the χ^2 test using the binned data from the masked simulations are shown in the lower panels. In both energy ranges, the unmasked maximum likelihood method indicates the presence of some non-uniform emission, but places its location a degree or more away from the simulated source location. The masked technique places the most likely source location within 0.05 degrees of the simulated location in both energy ranges.

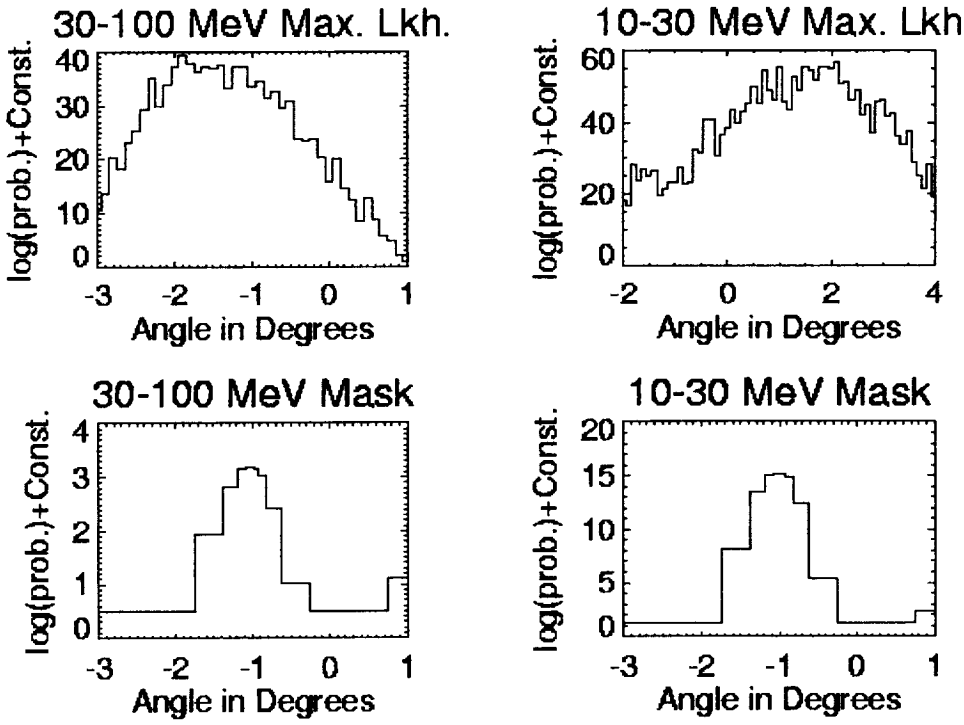

FIGURE 8. Source localization probability for masked (bottom) and unmasked (top) instruments.

The pair-tracking angular resolution of SIFTERCAM at lower photon energies (σ~10°) will allow us to localize Galactic diffuse emission and atmospheric background to angular regions covering ~0.1 sr. We find that the SIFTERCAM system observing a 0.1 sr angular area of the Galactic ridge would observe ~28×10^6 diffuse Galactic photons in a one year in the 30–100 keV range. A point source at 1% of the Galactic diffuse level would produce 2.8×10^5 detected photons in this energy range. The situation improves somewhat in the 10–30 MeV range where ~70×10^6 Galactic photons will be observed for the same angular extent and duration. A source at 1% of the Galactic diffuse flux produces 7×10^4 detected photons in this energy range.

At these low energies the pair-tracking angular resolution is not good enough to produce accurate source locations without the mask pattern information. Our preliminary simulations indicate that the SIFTERCAM mask approach provides more than an order of magnitude improvement over conventional, unmasked, pair telescopes. At higher energies, the angular resolution of the fiber tracker, rather than the mask, will begin to dominate the point source resolution, however the mask pattern's sensitivity to the difference between localized and truly point source emission will still be valuable.

REFERENCES

Carter, J., et al., "High resolution gamma ray telescope using a coded aperture mask and drift chamber," *MNRAS*, **198**, 33 (1982).

Jenkins, T. L., et al., "Modeling a High energy Gamma Ray Telescope," *Proc. 19th Intl. Cosmic Ray Conf., La Jolla*, **3**, 311 (1985).

Pendleton, G. N., et al., "FiberGLAST: a scintillating fiber approach to the GLAST mission," *Proc. SPIE*, **3765**, 12P (1999).